Rock Mech Rock Eng (2016) 49:4125–4135
DOI 10.1007/s00603-016-1032-y

ORIGINAL PAPER

Evaluation of Flooding Induced Seismicity from the Mining Area Schlema/Alberoda (Germany)

Holger Schütz[1] · **Heinz Konietzky**[1]

Received: 27 October 2015 / Accepted: 13 June 2016 / Published online: 4 July 2016

Abstract A dataset of 1653 seismic events recorded during flooding the mine area Schlema/Alberoda has been analyzed. The magnitude range was between ML = −2.5 and ML = 1.8. The results show a clear relation between triggered seismicity and flooding process. The Gutenberg–Richter law was used to predict a maximum magnitude for this area. Furthermore, seismological source parameters have been calculated. The measured peak ground velocities have been used to determine a prediction law which allows predicting peak ground velocities for hypothetically hypocenters in that area based on assumed source depth and magnitude.

Keywords Induced seismicity · Fluid-triggered seismicity · Peak ground velocity

1 Introduction

The uranium mine Schlema-Alberoda was operated near the town Aue in south-east Germany between 1947 and 1990 under the leadership of a joint venture between the former German Democratic Republic (GDR) and the former Soviet Union (USSR). The mine has reached a depth of about 2000 m below surface and is the deepest mine all over Europe. 49.5 Mio t of rock have been excavated, and 80,500 t Uranium ore was mined. In 1979, a seismic event with local magnitude of $M_L = 2.9$ and intensity MSK = 5 (Medwedew–Sponheuer–Karnik scale) was monitored close to the mining area. Due to this event and observations of underground dynamic destressing, a local seismic network was installed and extended within the following years. Seismic events were routinely located, and source parameters for selected events were determined (Konietzky 1990; Konietzky 1990–1991). It was found that most of the sources of the dynamic events are located outside of the mine inside the neighboring granitic intrusion. During the period of active mining, continuous online evaluation of seismic events was performed in conjunction with online hazard evaluation (Konietzky 1990–1991).

In 1990, the controlled flooding of the mine was started. A total excavated volume of 35 Mio m^3 had to be flooded. The flooding was finished in 2012. The flooding process was continuously monitored with a seismic network over the whole period of 22 years. This large dataset has been used for statistical calculations, correlations between seismicity and flooding level, numerical model calibrations and ground velocity predictions.

2 Geological and Geomechanical Situation

The uranium ores were mined in schistose layers at the flanks of a granitic intrusion as illustrated in Fig. 1. The tectonic structure is characterized by a big fault called 'Roter Kamm' and conjugated smaller faults crossing at 45°–90°. The conjugated faults are well known inside the schistose formation and penetrate several 100 m into the granite body.

In situ stress measurements in the mine performed by overcoring and hydraulic stress measurements indicate a quite anisotropic stress state, which is different in the two geological formations as shown in Table 1. Complex numerical stress field modeling performed recently (LfULG 2010) has confirmed these results. Deformation

✉ Holger Schütz
Holger.Schuetz@ifgt.tu-freiberg.de

[1] Geotechnical Institute, TU Bergakademie Freiberg, Gustav-Zeuner-Street 1, 09599 Freiberg, Germany

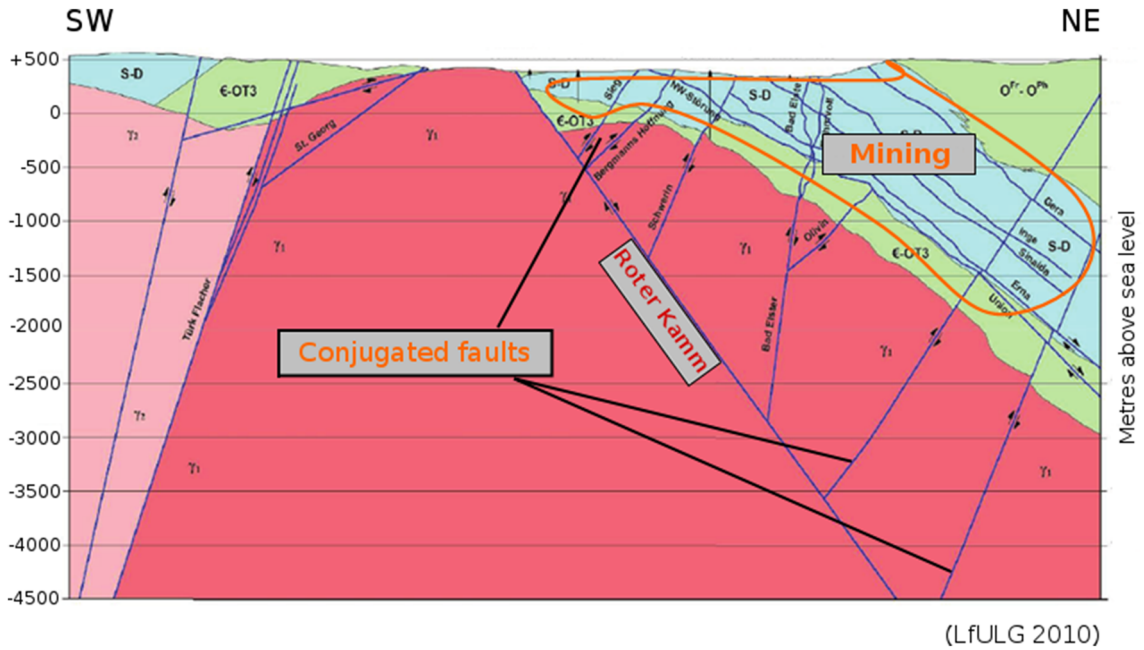

Fig. 1 Geological cross section with indication of mined area, granite intrusion (*red*), ordovician schist (*green*) and devonian schist (*blue*) (color figure online)

Table 1 Virgin in situ stress field in the mine at a depth of about 1500–2000 m below surface (Konietzky 1990–1991; LfULG 2010)

Principal stress component	Strike	Magnitude inside schist (MPa)	Magnitude inside granite (MPa)
σ_1	NNW	70–100	120–140
σ_2	NEE	50–60	45–60
σ_3	Vertical	25–40	20–30

measurements and detailed analysis of the seismoacoustic activities indicate that the granitic pluton relaxes in direction toward the schistose rock formation, where the mining operations took place. As data show, the stress anisotropy is quite high, especially inside the granite body.

3 Seismic Monitoring Network

The seismic monitoring was conducted by the Wismut company using the seismic monitoring system SÜA-3 with app. 40 stations [mainly one-dimensional geophones (vertical direction), but also two three-dimensional geophones and one hydrophone] positioned at the surface and underground (Wismut-NET shown in Fig. 2). The geophones have an eigenfrequency of 4.5 Hz and allow registering up to 400 Hz. The TU Bergakademie Freiberg has also installed a network (TUBAF-NET) at the surface above the mine with eight three-dimensional seismometers. The TUBAF seismometers have an eigenfrequency of 1 Hz and allow registering up to 100 Hz. In the time span between begin of 1993 and end of 2012 the Wismut-NET has recorded 1653 events and the TUBAF-NET 325 events. The regional network SX-NET operated by the University Leipzig also recorded seven events in the mine, which allows the calibration of local magnitudes with the regional network.

With this large number of events recorded by many stations, it was possible to perform a detailed analysis in terms of source location, source parameter determination and magnitude determination. The localization of the events was conducted with the modified location algorithm "multiMW" (Künzel 2013). The accuracy of located events specified by (Künzel 2013) is shown in Table 2.

4 Monitoring Results

Figure 3 shows an overview of 1426 located seismic events until 2012. It is clearly visible that the main activity takes place in the granite (1315 events). In the schist formations, only 111 events with small local magnitudes (M_L) were detected.

A classification of seismic source regions used by the Wismut company (Wallner 2009) is shown in Fig. 4. The numbering corresponds to the sequence of first detection. First activities were recorded in the red part (Herd 1 a,b), and later activities spread outwards. Figure 5 shows that the first

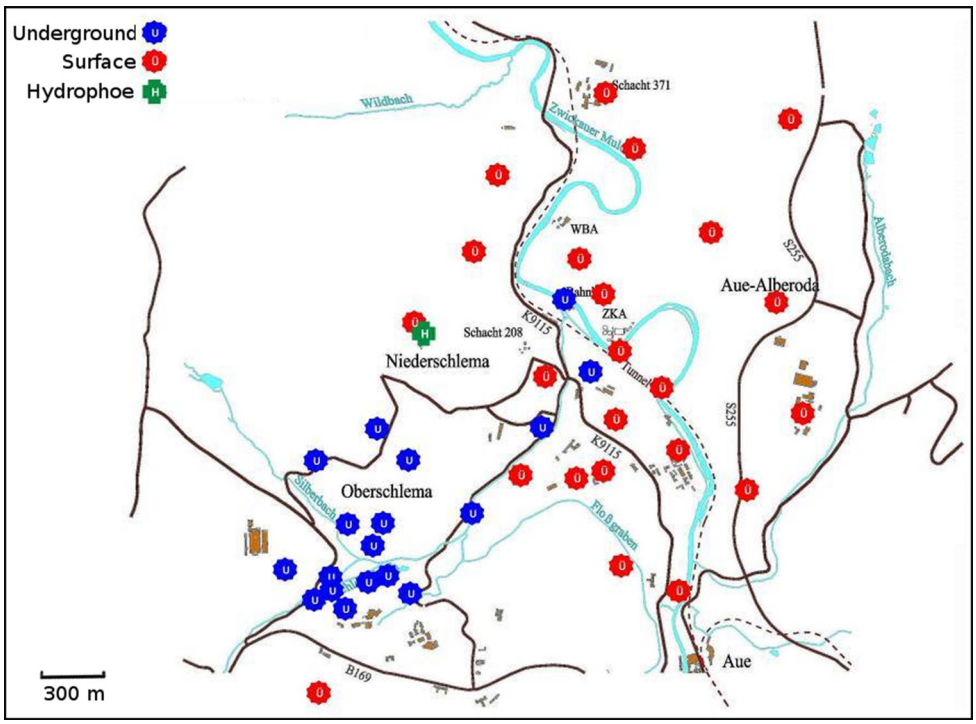

Fig. 2 Wismut-NET (Wallner 2009)

Table 2 Location accuracy in the 95 % confidence interval (Künzel 2013)

Δ Latitude (m)	Δ Longitude (m)	Δ Depth (m)
29.1	38.4	62.7

source areas are the deepest and become shallower with higher number. That the source areas are very likely connected to fault systems is illustrated in Fig. 5. Unfortunately, the faults in the granite were not investigated in detail because the granite was not target of the mining activities.

All source parameter calculations are based on the Madariaga model for a circular fault (Madariaga 1976). This model was chosen because of simplicity (only one geometrical fault parameter: radius) and the possibility for comparison with results of previous works. Source parameters have been determined based on spectral corner frequencies and spectral seismic moment. For the scalar seismic moment M_0, Eq. (1) is used.

$$M_0 = \frac{4 \cdot \pi \cdot \rho \cdot r \cdot v_p^3 \cdot \Omega_0}{\Theta} \tag{1}$$

Ω_0 is determined from the low-frequency flat amplitude level of the displacement-frequency spectrum of the P-waves. The distance between source and observation point r can be determined after localization of the event. Rock density ρ and P-wave velocity V_P have been determined from other observations with $\rho = 2850$ [kg/m^3] and $V_P = 5200$ [m/s], respectively. The directivity correction factor Θ was assumed as a constant with a value of 0.8 because fault plane solutions could not be performed in most cases.

As described in (Hurtig and Stiller 1984), the source radius R is given by Eq. (2) where $f_{c,P}$ is the spectral corner frequency of the P-wave.

$$R = \frac{2.07 \cdot v_P}{\left(2 \cdot \pi \cdot f_{c,P}\right)^2}. \tag{2}$$

The dislocation D is given by Eq. (3) applying the shear modulus $\mu = 2.565 \times 10^{10}$ [N/m^2].

$$D = \frac{M_0}{\mu \cdot \pi \cdot R^2}. \tag{3}$$

The stress drop $\Delta\sigma$ was calculated by Eq. (4).

$$\Delta\sigma = \frac{7 \cdot M_0}{16 \cdot R^3}. \tag{4}$$

The predictions showed in Figs. 6 and 7 were determined from linear regressions in which the Y-axis was plotted in logarithmic scale and transformed back to non-logarithmic scale. Figure 8 shows the calculated stress drop. The values scatter a lot and there is no dependency from the magnitudes visible.

5 Geomechanical Interpretation

The excellent seismic database allows deducing the Gutenberg–Richter relation according to Eq. (5) where N is the number of events having a magnitude $\geq M_L$. Figure 9

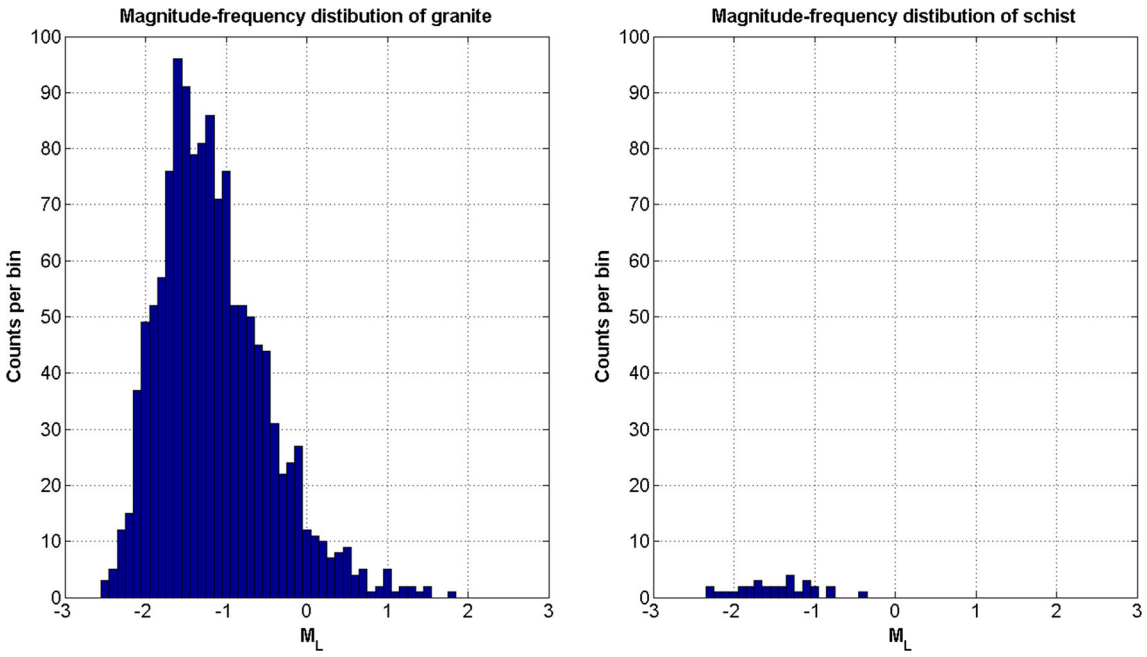

Fig. 3 Magnitude-frequency distributions for events located in granite (*left*) and schist (*right*)

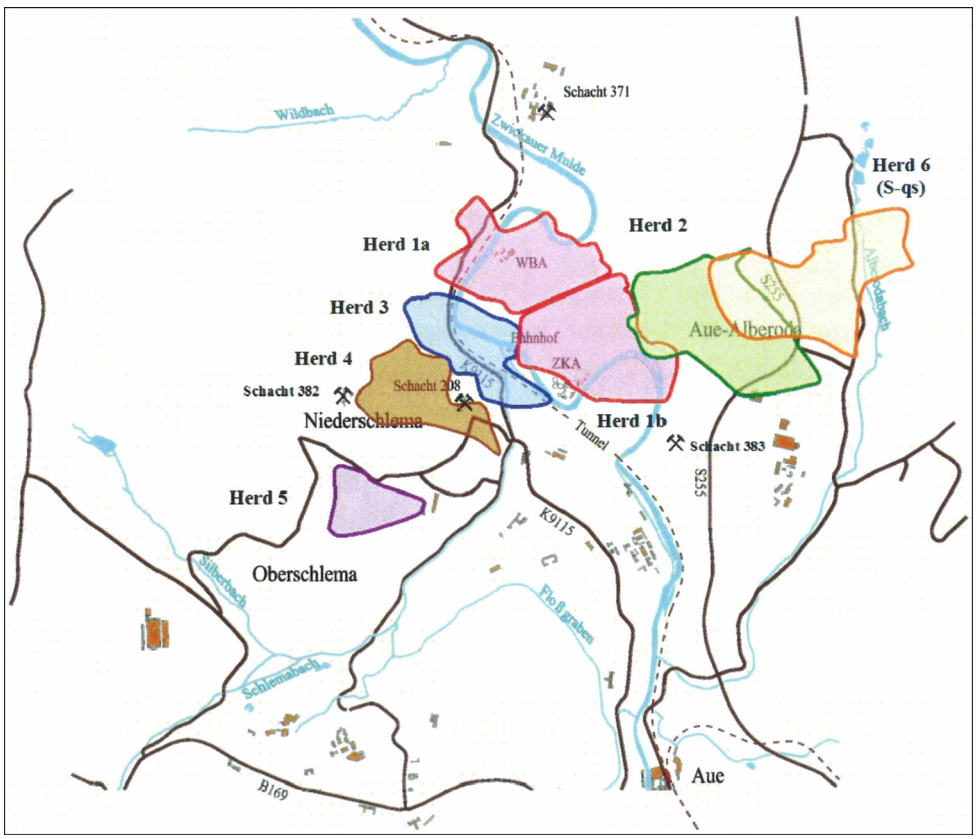

Fig. 4 Source area classification after WISMUT (Wallner 2009)

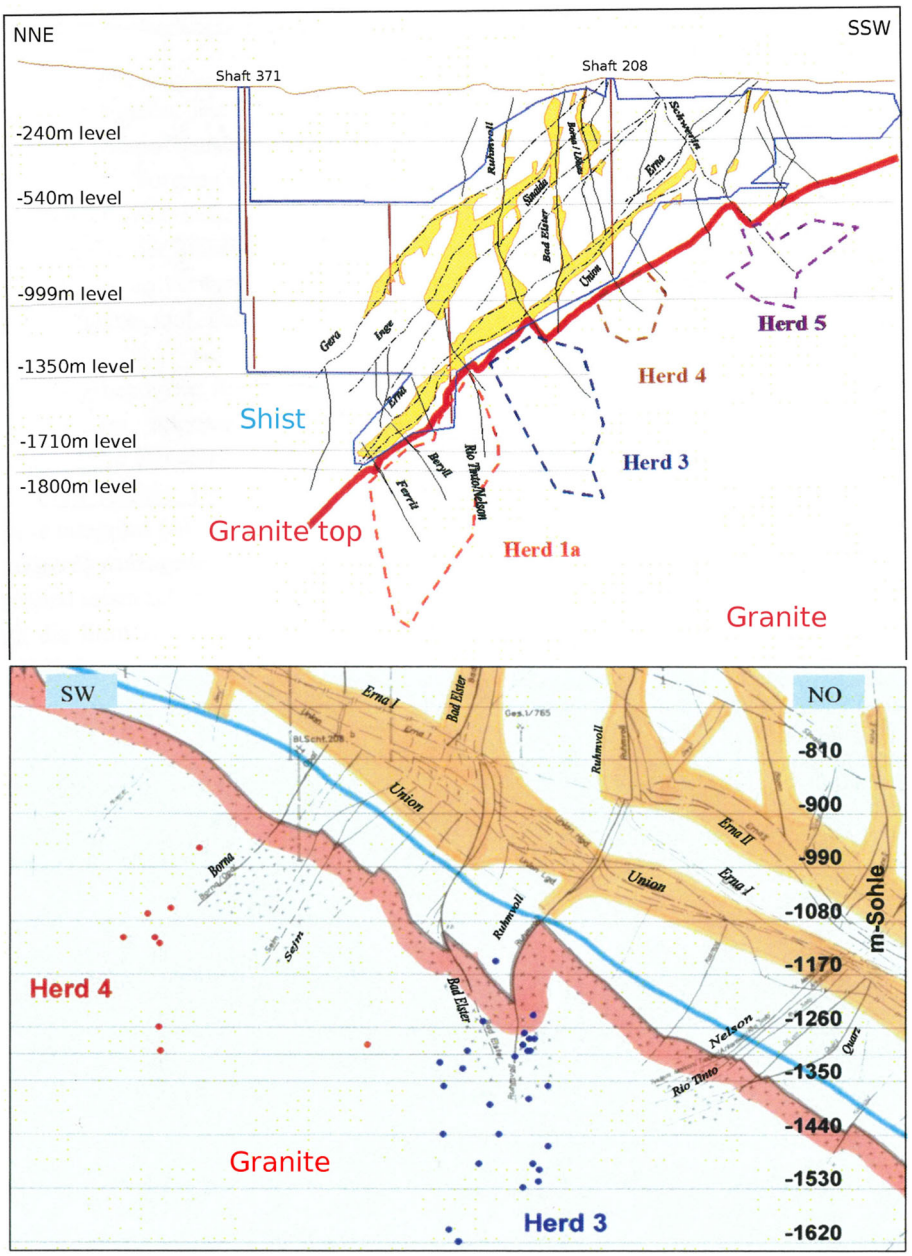

Fig. 5 Geological cross sections with location of recorded events, *above* overview plot of source regions, *below* detailed plot indicating individual events (*blue dots*) (Wallner 2009) (color figure online)

shows the magnitude frequency distributions and the Gutenberg–Richter law for events located inside the granite and the schist.

$$\log_{10} N = a - b \cdot M_{\mathrm{L}} \tag{5}$$

The maximum local magnitude inside the schistose formation is much smaller and will not exceed 0. Due to the fact that only about 100 events were located inside the schist, the Gutenberg–Richter law is—from the statistical point of view—not very reliable. But clearly visible, the slopes of the curves for granite and schist are different. These slopes correspond to the so-called b value of the Gutenberg–Richter law.

For the schist and granite, b values of 1.5 and 0.82, respectively, were determined. The differences can be explained by the lower brittleness of the schist compared to the granite, which leads to more induced events with smaller rupture areas in the granite and consequently to smaller magnitudes for the schist. Down to a local magnitude $M_{\mathrm{L}} = -1$, the recordings can be considered as complete. The maximum magnitudes deduced from the Gutenberg–Richter law are $M_{\mathrm{L}} = -0.4$ for the schist and $M_{\mathrm{L}} = 2.4$ for the granite. So far, the maximum measured magnitude over a period of about 25 years is $M_{\mathrm{L}} = 1.8$. This event was located inside the granite body.

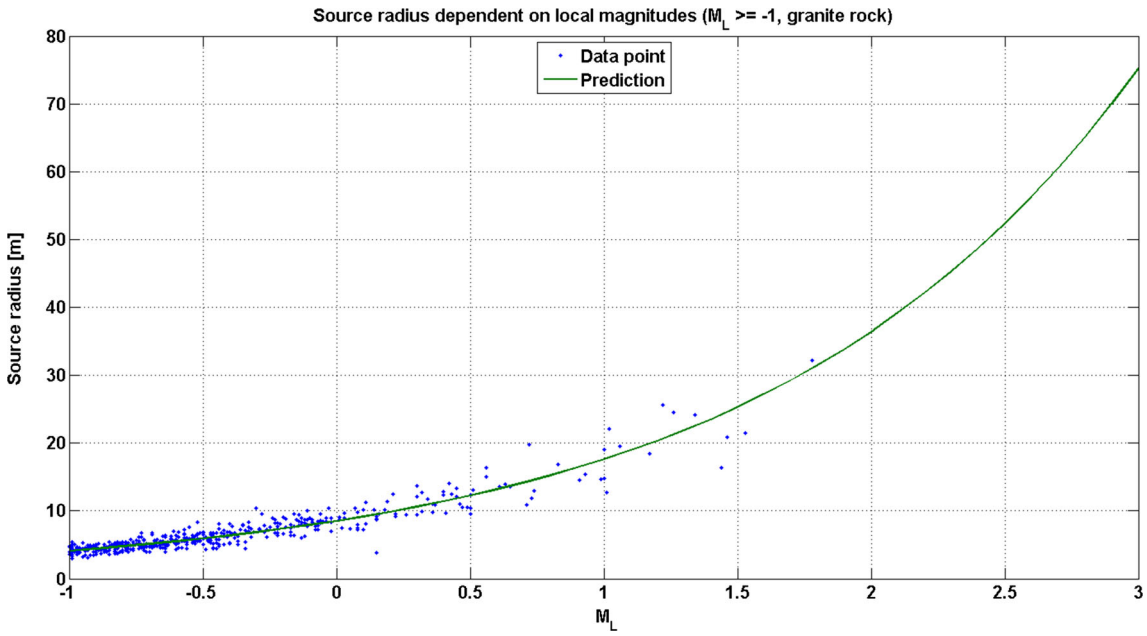

Fig. 6 Source radius dependent on local magnitudes for $M_L \geq -1$ and with hypocenters in granite rock

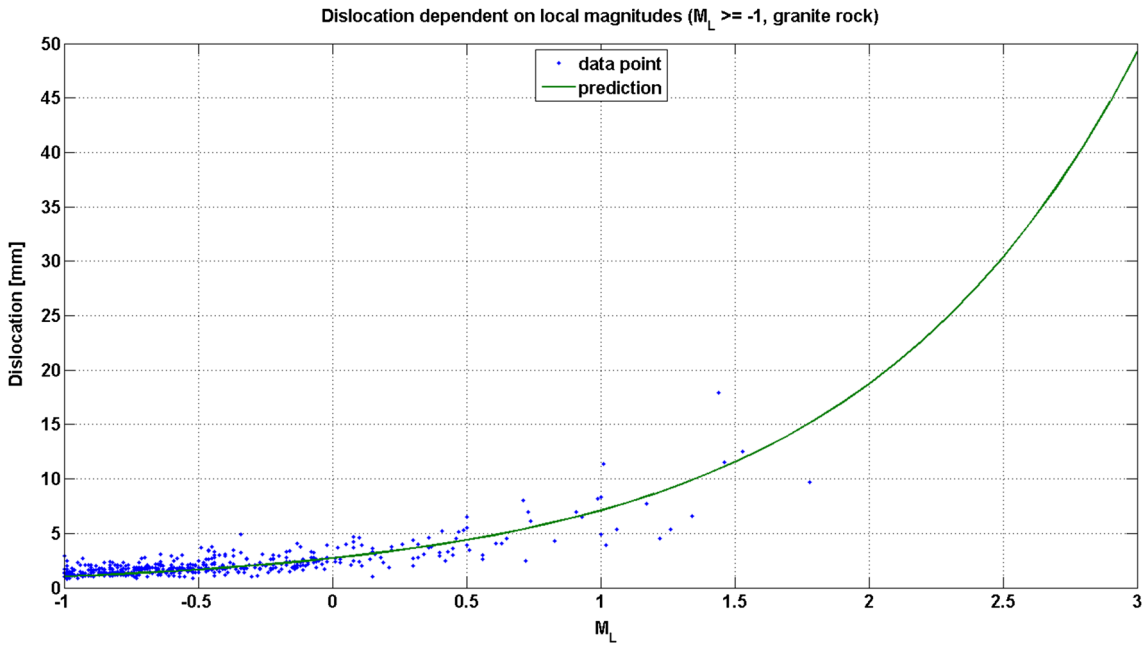

Fig. 7 Dislocation dependent on local magnitudes for $M_L \geq -1$ and with hypocenters in granite rock

To investigate the influence of the flooding, several correlations have been investigated. Figure 10 shows two of them. It is clearly visible, that the cross-correlation of hydrostatic pressure and cumulative seismic energy (blue line) has a nearly perfect correlation with a correlation factor of Cf = 0.99 and the time offset is zero. This means the system reacts immediately or at least on the same day. Because we have only one measured value per day for the flooding level, the temporal resolution is limited to 1 day. The cross-correlation of pressure change and seismic energy (green line) is not that clear. The best correlation with a correlation factor of Cf = 0.47 is observed for a time offset of 43 days, which means that the system reacts with an average delay of 43 days. One should take into account that pressure perturbations along fault/fracture systems take some time, and water paths are quite complex

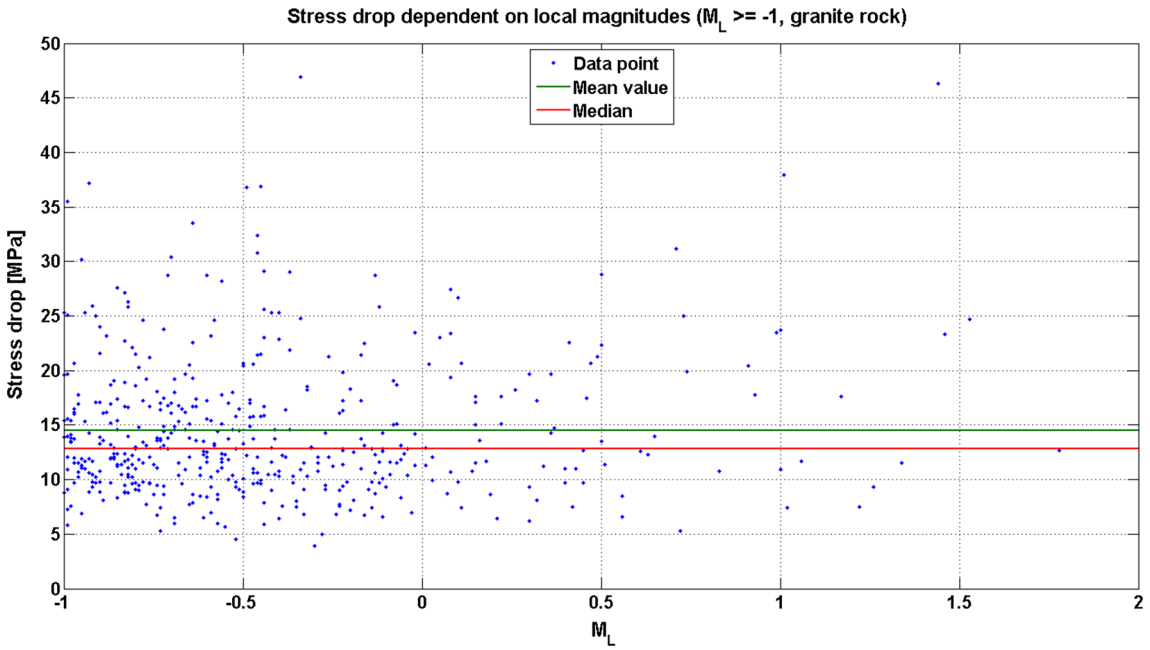

Fig. 8 Stress drop dependent on local magnitudes for $M_L \geq -1$ and with hypocenters in granite rock

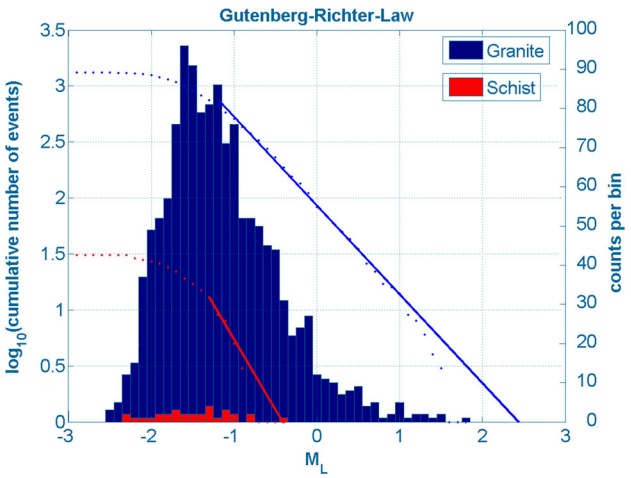

Fig. 9 Gutenberg–Richter law and magnitude frequency distribution

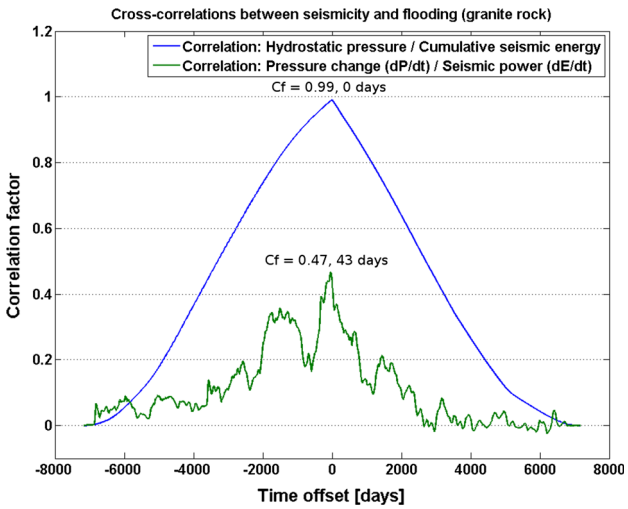

Fig. 10 Correlations between seismicity and flooding for hypocenters in granite rock

and different at any location. This is probably the explanation for the bad correlation or in other words, each seismic event seems to be connected to a different hydro-mechanical situation. Also, the hydraulic impact of precipitation (rainfalls and melting of snow) might have an additional influence.

The basic physical mechanism behind the induced seismicity is the increase of joint (pore) water pressure in favorable oriented joint systems. The increasing water level due to flooding generates increasing joint (pore) water pressure, which leads to reduced effective stresses and consequently triggering of slip and fracturing, respectively, along these discontinuities. This explanation is supported not only by correlation between location of seismic events and geological structures, but also by fault plane solutions.

6 Engineering Seismological Investigations

The German standard DIN 4150 (DIN 1999) specifies limit values for buildings to avoid damage on them. These values are given as peak ground velocities (PGV) specified for different frequencies and different building types. A PGV value of 3 mm/s is specified for most sensitive buildings

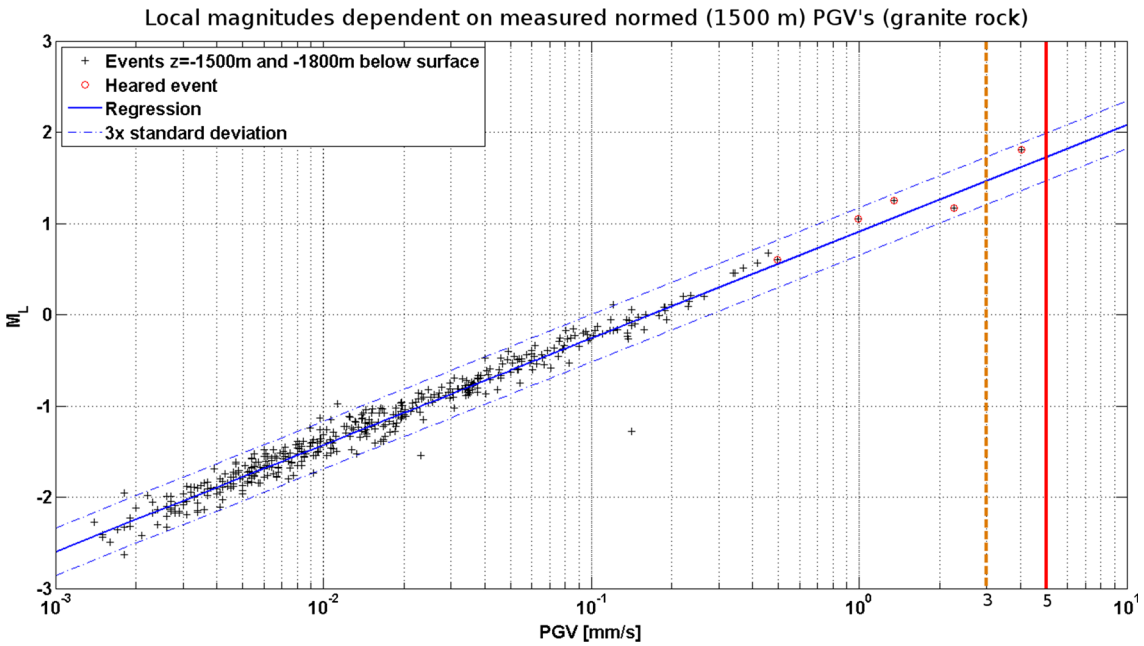

Fig. 11 PGV for events in granite rock (*vertical red/orange lines* indicate limits according to DIN 4150/3) (color figure online)

Fig. 12 Estimation of damping parameter (example)

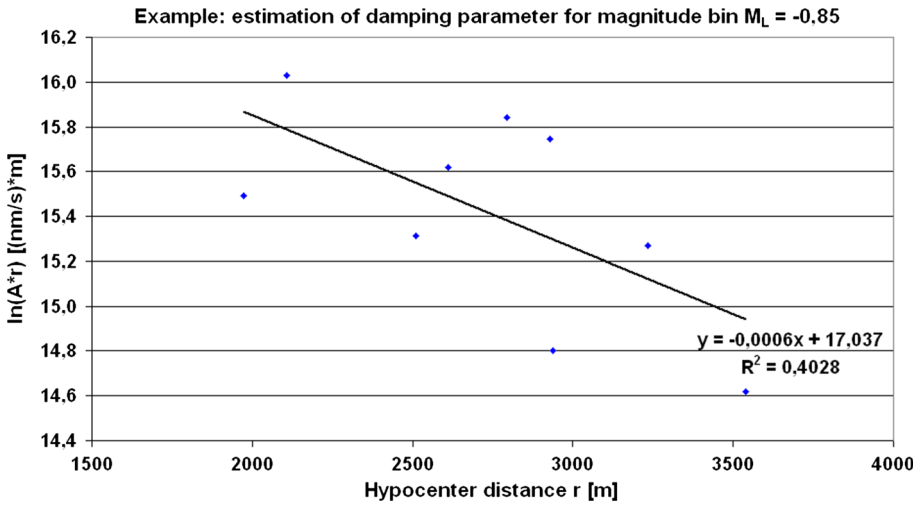

(e.g., historical buildings), and 5 mm/s is specified for residential buildings and 10 mm/s for industrial buildings. All previous values are valid for a frequency range below 10 Hz, which is also typical for induced seismicity. Figure 11 shows the distance normalized PGV's of seismic events in the granite. Red events where noticed by people. Such events have a magnitude of about $M_L \geq 0.6$ and a PGV ≥ 0.5 mm/s.

In order to predict the PGV's, an approach was developed, which is based on several assumptions explained below. For a spherical wave the reduction in amplitude is given by Eq. (6). The damping parameter α is defined as given by Eq. (7).

$$A = A_0 \cdot e^{-\alpha \cdot r} \cdot \frac{1\,[m]}{r} \tag{6}$$

$$\alpha = \frac{\pi \cdot f}{Q \cdot v_{P,S}} \left[m^{-1}\right] \tag{7}$$

where A is the amplitude at the observation point, A_0 is the amplitude at the origin, r is the distance between origin and observation point, α is the damping coefficient, f is the frequency, Q is the seismic quality factor and $V_{P,S}$ are the compression wave and shear wave velocities, respectively.

The exponential term describes the intrinsic damping and the term $\frac{1}{r}$ the geometrical damping. The values for A, r and α were obtained from the seismological registrations

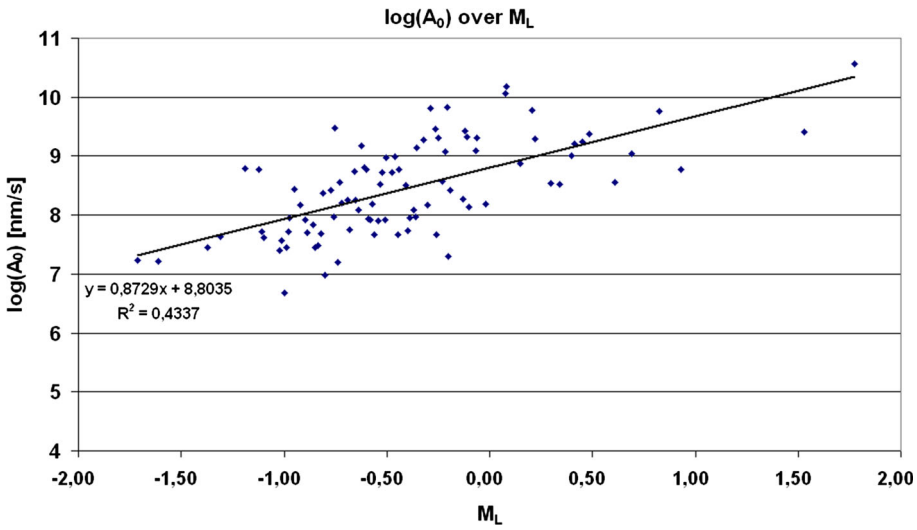

Fig. 13 Estimation of $\log(A_0)$ dependent on local magnitudes

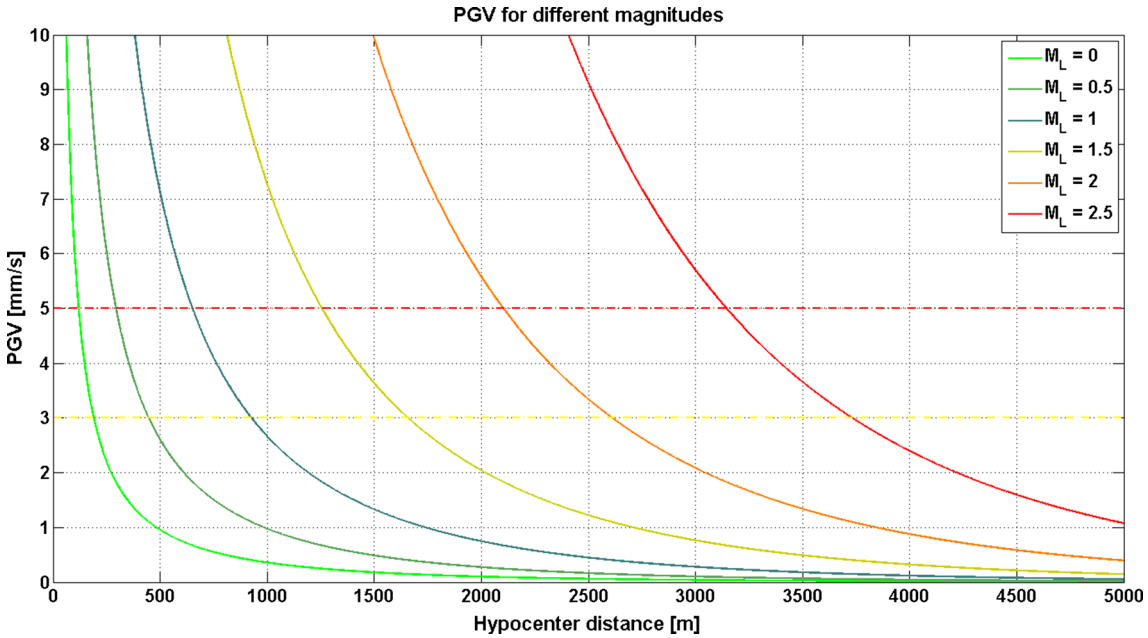

Fig. 14 Calculated PGV's for different magnitudes (*dashed lines* are limits according to DIN 4150/3)

for individual magnitude classes. Therefore, Eq. (6) can be re-written in the following manner:

$$\ln(A \cdot r) = -\alpha \cdot r + \ln(A_0) \tag{8}$$

A subsequently performed regression analysis delivers A_0 and α for each magnitude in the range of $M_L = -1.7$ and $M_L = 1.8$ (see example in Fig. 12 for one magnitude). The results for A_0 were plotted versus corresponding magnitudes. A subsequently performed regression analysis delivers Eq. (9), which is illustrated in Fig. 13.

$$A_0 = 10^{0.8729 \cdot M_L + 8.8035} \tag{9}$$

Then, the damping parameter α was averaged for all magnitude bins (see Eq. (8) and Fig. 12). Equation (6) can be re-written considering Eq. (9) and the averaged damping parameter:

$$A = 10^{0.8729 \cdot M_L + 8.8035} \cdot e^{-0.000578 \cdot r} \cdot \frac{1}{r} \tag{10}$$

Because the measured values are peak ground velocities, A corresponds with PGV. Figure 14 shows several peak ground velocities calculated by Eq. (10) for distances between 0 and 5000 m and different local magnitudes. The

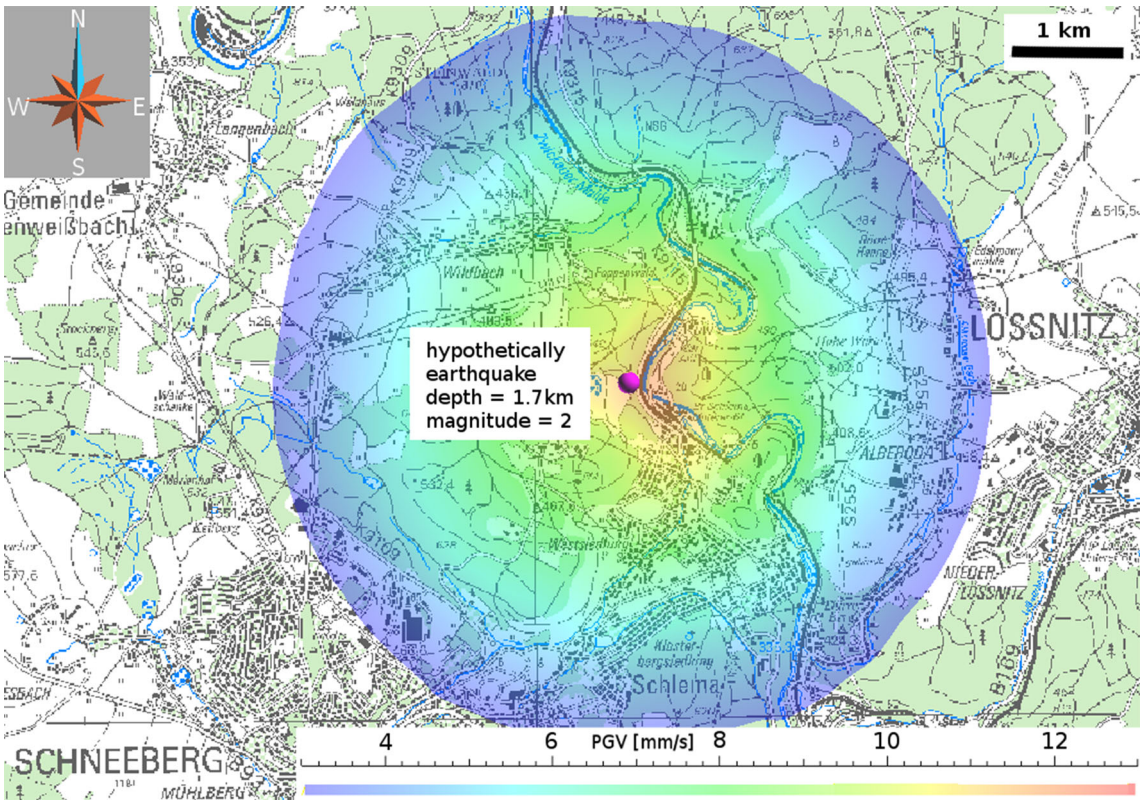

Fig. 15 PGV prediction for a hypothetically induced seismic event calculated on DEM

distribution of predicted PGV's at the surface can be shown on a map, like illustrated by Fig. 15. Because the investigated area is very mountainous a digital elevation model (DEM) was used to consider the influence of mountains and valleys. The magenta dot indicates the hypocentre at a depth of 1700 m below surface. The local magnitude is set to $M_L = 2.0$.

The proposed procedure allows the prediction of PGV at any point at the surface in dependence on local magnitude and source location. Nevertheless, the following limitations should be taken into account.

- Detailed radiation pattern of source is neglected (replaced by averaging).
- Damping factor is considered to be constant.
- Geological inhomogeneities are neglected.
- Local surface site effects are neglected.
- Equation (10) is valid only for the Aue/Schlema region.

7 Conclusions

Seismic events were triggered by the flooding process of the mine Aue/Alberoda due to increasing joint and pore water pressure at favorable oriented joints. A strong correlation between hydrostatic pressure and cumulated released seismic energy was discovered. Hypocenters are mostly connected to existing faults in the granitic rock formation. The Gutenberg–Richter relation was used to deduce the maximum magnitude. The maximum expected magnitude is $M_L = 2.4$ for granite and, with lower reliability, $M_L = -0.4$ for schist. Measured peak ground velocities and source parameters have been used to develop a prediction law for peak ground velocity. This law has been used to calculate PGV's on a DEM. Although the deduced specific correlations and formulas are only valid for the Aue/Schlema region, the general procedure can be applied and adopted to other regions too.

Acknowledgments The research work was founded by the German Federal Ministry for Environment (BMU) under the support code 0325191F and managed by Project Management Jülich (PTJ). The support of R. Mittag (seismological data interpretation, TU Bergakademie Freiberg), O. Wallner (geodetic interpretation, Wismut GmbH) and A. Hiller (geological information, Wismut GmbH) throughout the whole project is highly acknowledged.

References

DIN 4150/3 (1999) Erschütterungen im Bauwesen, Teil3, Einwirkung auf bauliche Anlagen, Deutsches Institut für Normung e.V. Beuth Verlag, Berlin

Hurtig E, Stiller E (1984) Erdbeben und Erdbebengefährdung. Akademie-Verlag, Berlin

Konietzky H (1990) Classification of seismic events in a mining area in the Erzgebirge mountains of the GDR. In: Gerlands Beiträge Geophysik, Nr. 99-2, S.169–174

Konietzky H (1990–1991) Locating of seismic sources in rock masses and the determination of source parameters. In: Gerlands Beiträge Gephysik, Nr. 99-1, S.44–53

Künzel U (2013) Seismizität im Umfeld der Uranerzlagerstätte Schlema-Alberoda und modifizierte Auswertemetthoden für eine präzise Lage- und Stärkeermittlung der im Nahfeld instrumentell registrierten Beben. Veröffentlichungen des Institutes für Geotechnik der TU Bergakademie Freiberg, Heft 2013-1

LfULG (2010) Forschungsbericht Tiefengeothermie Sachsen. Landesamt für Umwelt, Landwirtschaft und Geologie, Freiberg

Madariaga R (1976) Dynamics of an expanding circular fault. Bull Seism Soc Am 65:163–182

Wallner O (2009) Analyse bergbauinduzierter Bodenbewegungen und Seismizität während der Gewinnungs- und Flutungsphase einer komplexen Gangerzlagerstätte. Dissertation, Institut für Markscheidewesen und Geodäsie, TU Bergakademie Freiberg